ACS Catalysis

RESEARCH ARTICLE

pubs.acs.org/acscatalysis

Subnanometer Palladium Particles Synthesized by Atomic Layer Deposition

Hao Feng,[†] Joseph A. Libera,[‡] Peter C. Stair,[†,§] Jeffrey T. Miller,[†] and Jeffrey W. Elam*[,‡]

[†]Chemical Science and Engineering Division and [‡]Energy Systems Division, Argonne National Laboratory, Argonne, Illinois 60439, United States

[§]Department of Chemistry, Northwestern University, Evanston, Illinois 60208, United States

ABSTRACT: Monodispersed palladium nanoparticle catalysts were synthesized by atomic layer deposition (ALD) using alternating exposures of Pd hexafluoroacetylacetonate ($Pd(hfac)_2$) and formalin on an alumina support. The size of the ALD Pd particles could be tuned by adjusting the preparation conditions. Conventional ALD conditions produced Pd particles with an average size of 1.4 nm. Removal of surface hydroxyls from the alumina support by a chemical treatment using trimethyl aluminum (TMA) before performing Pd ALD led to nanoparticles larger than 2 nm. Ultrasmall (subnanometer) Pd particles were synthesized using low-temperature metal precursor exposures, followed by applying protective ALD alumina overcoats. The ALD Pd particles were characterized by transmission electron microscopy, extended X-ray absorption fine structure, and diffuse reflectance infrared Fourier transform spectroscopy techniques. The Pd loadings were measured by X-ray fluorescence. The catalytic performance of ALD Pd particles of different sizes was compared in the methanol decomposition reaction. The specific activity (normalized by Pd loading) of the ultrasmall Pd particles was higher than those of the larger particles. Considering the metal dispersion factor, the turnover frequency (TOF) of the ultrasmall Pd particles is comparable to that of the medium-sized (1.4 nm, on average) Pd particles synthesized under standard ALD conditions. The large Pd particles (>2 nm) are a factor of 2 less active than the smaller Pd particles.

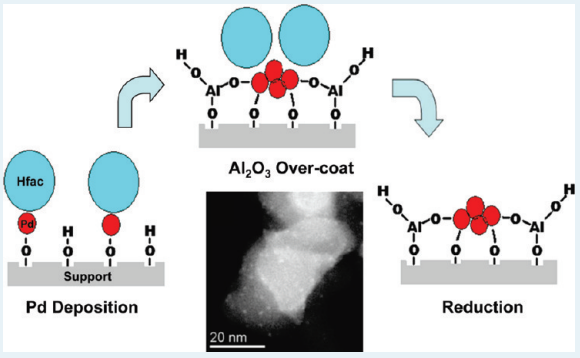

KEYWORDS: palladium (Pd) particles, atomic layer deposition (ALD), nanoparticle catalyst

INTRODUCTION

In a number of heterogeneous and electrocatalytic reactions, the size of the catalyst particles plays a major role in determining the catalytic performance.[1−8] Therefore, a synthesis method that can precisely tune the composition and morphology giving uniform and subnanometer-sized metallic nanoparticles could lead to significant improvements in catalytic performance. In addition, nanoparticles of identical composition, but which differ in average particle size, will provide the opportunity to better investigate the fundamental issues associated with particle size effects in catalytic reactions. Conventional methods of synthesizing noble metal catalysts, such as precipitation or impregnation, usually lead to a broad particle size distribution (particle dimensions spread over a range of several nanometers to tens of nanometers), with average diameters of ∼1 nm and larger.[9,10] Because of this, many new synthetic approaches have been developed to produce monodispersed noble metal nanoparticles by enclosing the metal precursors in a confined space, such as in micelles or reverse micelles, microemulsions, dendrimers, or functionalized polymers.[11−19] These preparation methods are usually relatively expensive and have limited scalability and flexibility. Moreover, the harsh treatments used to remove the stabilizing ligands often lead to particle sintering.

Atomic layer deposition (ALD) has recently been demonstrated as an effective method for synthesizing supported, metallic nanoparticle catalysts.[20−25] In the ALD process, two gaseous precursors are pulsed alternately such that each reacts in a self-limiting fashion with the surface functional groups generated by the previous pulse. ALD allows the precise, conformal deposition of a wide variety of materials onto nearly any substrate, including the high-surface-area support materials widely used in heterogeneous catalysis.[26] One of the attractions of ALD for catalyst synthesis is that it offers the potential for commercial viability, as demonstrated by the successful implementation of ALD technology in semiconductor manufacturing.[27]

Generally, it is difficult to achieve thin, continuous noble metal films by ALD on oxide surfaces due to the relatively slow chemisorption kinetics of the ALD metal precursor and the diffusion and sintering of the noble metal species. As a result, thin ALD noble metal deposits typically consist of islands or agglomerates, usually in the nanometer-sale. Such nucleation phenomena during the early stage of noble metal ALD film growth can be employed to synthesize nanoparticles. Due to the self-limiting

Received: February 19, 2011
Revised: April 13, 2011
Published: April 25, 2011

Table 1. Summary of ALD Pd Sample Preparation Procedures, Elemental Pd Analysis, Pd Dispersion (calculated using the model developed by Fritsche et al. and by Montejano-Carrizales et al.[42,43]), and Estimate of the Average Pd Particle Size and Standard Deviation by TEM

	support hydroxyl removal			ALD modifications					
sample	thermal treatment	EtOH	TMA	low-*T* ALD	ALD overcoating	wt % Pd	estimated dispersion[a]	av TEM particle size (nm)	standard deviation (nm)
1	–	–	–	–	–	1.6	0.64 ± 0.04	1.4	0.4
2	yes	–	–	–	–	1.2	0.66 ± 0.04	1.4	0.3
3	–	–	yes	–	–	0.9	0.50 ± 0.03	2.2	0.3
4	–	–	–	yes	–	1.7	0.72 ± 0.04	1.2	0.3
5	–	–	–	–	yes	1.6	0.77 ± 0.04	1.1	0.3
6	–	–	–	yes	yes	1.9	0.85 ± 0.03	0.8	0.2
7	–	yes	–	yes	yes	1.2	0.84 ± 0.03	0.8	0.2

[a] The error estimation is based on the uncertainty in particle size determination from TEM images, which have a resolution of ~0.1 nm.

nature of the surface reactions in ALD, metal particles synthesized by ALD are highly dispersed. In addition, the layer-by-layer approach enables precise control over the particle size. Since the ALD catalyst particles are deposited directly on the support, no postsynthesis treatment is required.

Research on ultrasmall (<1 nm) catalyst particles is of particular interest due to their unique catalytic properties;[28,29] however, the synthesis and stabilization of monodispersed, ultrasmall noble metal particles in meaningful quantities remains a challenge. ALD usually generates noble metal particles with dimensions of 1−2 nm or larger. However, by modifying the ALD process conditions and the initial state of the substrate surface, it may be possible to further reduce the particle size. Herein, we report the use of modified ALD methods to synthesize ultrasmall Pd particles. By varying the preparation conditions, the average size of the ALD Pd particles could be tuned in the range of ~0.8 to ~2.2 nm with a narrow size distribution. The catalytic performance of the ultrasmall Pd particles was evaluated in methanol decomposition. In this reaction, the high catalytic activity of the ultrasmall catalyst particles correlated with their dispersion.

EXPERIMENTAL SECTION

The supported Pd nanoparticle catalysts were synthesized on a silica gel powder (Silicycle S10040M, 99.6 m^2/g) coated with five cycles of ALD alumina. The ALD of alumina and Pd were carried out using methods published previously.[20,26] Specifically, alumina ALD was performed in a viscous flow reactor using alternating exposures to trimethyl aluminum (TMA, Aldrich, 99%) and deionized water using precursor exposure and purge times of 60 s at 1.0 Torr.[30] The Pd ALD used alternating exposures to palladium hexafluoroacetylacetonate ($Pd(hfac)_2$, Aldrich, 99.9%) and formalin (Aldrich, 37% HCOH and 15% CH_3OH in aqueous solution) with 400 s exposure and purge times. Ultrahigh-purity nitrogen (Airgas, 99.999%) was used as the purge gas. The $Pd(hfac)_2$ precursor was held in a stainless steel bubbler kept at 60 °C, and the other precursors were used at room temperature. Only one Pd ALD cycle was performed to synthesize the catalyst samples to minimize the Pd particle size.

We evaluated a number of methods to synthesize ultrasmall Pd particles: (1) pretreatments to remove alumina surface hydroxyl groups, including thermal annealing, reaction with alcohols to form surface alkoxides, and treatment with TMA; (2) lower temperature $Pd(hfac)_2$ precursor exposures; (3) ALD alumina overcoating; and (4) combinations of these methods. The methods used to synthesize the Pd samples for this study are summarized in Table 1.

For some of the samples, the alumina surface hydroxyls were partially dehydrated by heating or chemically treated to produce surface alkoxide groups. The thermal dehydration was carried out in an internal heating stage positioned within the hot-walled ALD reactor to facilitate rapid heating and cooling. The stage encompassed a metal tray to hold the powder, heating rods, and a K-type thermocouple enclosed inside the bottom of the tray. During the annealing process, the alumina-coated silica gel was heated to 600 °C in a flow of N_2 and was held at this temperature for 2 h before cooling to 200 °C to carry out the Pd ALD.

The chemical dehydroxylation treatments consisted of exposures to either TMA or ethanol vapor. The TMA exposures were intended to convert surface hydroxyls into $O-Al(CH_3)_2$ species, which are not reactive toward the $Pd(hfac)_2$.[31] Likewise, the ethanol chemical treatment will form nonreactive $O-CH_2CH_3$ surface species.[32−36] The TMA treatments used 120 s exposures to TMA vapor at 200 °C, followed by a 120 s N_2 purge, and the ethanol treatments used 120 s exposures to ethanol vapor at 100 °C, followed by a 400 s N_2 purge.

The low-temperature $Pd(hfac)_2$ precursor exposures were carried out at 100 °C, 1.0 Torr. After the metal precursor dose and purge, the ALD reactor was heated to 200 °C under N_2 purge, and then the formalin exposure and purge were performed. The ALD alumina overcoating was performed following the $Pd(hfac)_2$ exposure and purge. Two cycles of TMA/water were performed at the same temperature as the $Pd(hfac)_2$ exposures with the intention of forming a thin, protective layer to inhibit subsequent particle growth. Finally, the formalin exposures were performed following the alumina ALD.

X-ray fluorescence spectroscopy (XRF) was used as a nondestructive method to determine the Pd loading on the alumina-coated silica gel. The XRF spectra were measured with an Oxford Instruments ED2000, and the Pd loading was quantified using the Pd K lines. The XRF data were calibrated using an ALD sample of known Pd loading as determined by inductively coupled plasma atomic emission spectroscopy measurements.

Transmission electron microscopy (TEM) measurements were performed on a JEOL JEM-2010 system. The number of Pd particles in each TEM image was counted, and the sizes of these particles were determined by measuring the diameter of each particle against the scale bar in magnified prints of the

images. For each catalyst sample, more than 300 Pd particles in several different TEM images were measured.

X-ray absorption near edge spectroscopy (XANES) and extended X-ray absorption fine structure (EXAFS) measurements were made in transmission mode at the insertion-device beamline of the Materials Research Collaborative Access Team (MR-CAT) at the Advanced Photon Source located at Argonne National Laboratory. Data were collected in quick EXAFS mode in about 2 min. Pd foil was simultaneously collected for energy calibration of the Pd K edge (24.350 keV). After reduction in 10% H_2 at 250 °C, the ALD Pd samples were cooled to room temperature under He flow, and then the EXAFS spectra were recorded in a controlled atmosphere reactor without exposure to air. EXAFS data were extracted using WINXAS 3.1 software, and the coordination parameters were obtained using standard procedures; that is, least-squares fitting of the k^2 weighted magnitude and imaginary part of the Fourier transform of EXAFS oscillations. Pd−Pd phase and amplitude functions were obtained from experimental data on Pd foil, and the data range was Δk = 2.7−11.7 Å^{-1} and Δr = 1.7−2.7 Å.

Diffuse reflectance infrared Fourier transform spectroscopy (DRIFTS) measurements were performed using an ABB Bomen FTLA2000 instrument outfitted with a Harrick Scientific praying mantis accessory. Background spectra were acquired after purging the sample with ultrahigh purity (Airgas, 99.99%) argon for >100 min at a flow rate of ∼60 sccm. CO (0.25% Airgas, research grade) at a flow rate of ∼100 sccm was then introduced into the DRIFTS cell for 2 h. Drifts spectra of CO chemisorbed on the Pd samples were recorded using 600 scans with a resolution of 4 cm^{-1}.

The methanol decomposition reaction was carried out in a stainless steel microreactor with an inside diameter of ∼4 mm; 5−15 mg of the catalyst powder was used in each experiment. The catalyst was held in the middle of the reactor by a plug of quartz wool. A K-type thermocouple was positioned in contact with the catalyst layer to measure the temperature. Methanol vapor (∼4%) was introduced into the reactor using an argon (Airgas, 99.99%) gas bubbler kept at room temperature using a stream of pure argon as the balance gas. The total methanol/argon flow through the reactor was 10 sccm. The catalysis tests were carried out in the temperature range 230−270 °C at atmospheric pressure. The reaction products were analyzed using an HP 5890 gas chromatograph equipped with a thermal conductivity detector (TCD). Signals from the TCD were calibrated using certified standard gas mixtures (Scotty, 1.00% CO_2, 0.999% CO, 1.00% H_2, 0.998% CH_4, balance of nitrogen).

RESULTS AND DISCUSSION

Palladium ALD has been studied on alumina surfaces using alternating exposures to $Pd(hfac)_2$ and formalin at 200 °C. The reaction mechanism during the first ALD cycle is believed to be[34]

$$Al{-}OH^{*} + Pd(hfac)_2 \rightarrow Al - O - Pd(hfac)^{*} + Hfac \quad (1)$$

$$Al - O - Pd(hfac)^{*} + HCOH \rightarrow Al - O - Pd - Hx^{*} + Hfac + CO + 0.5(1 - x)H_2 \quad (2)$$

In this mechanism, the $Pd(hfac)_2$ precursor first reacts with the surface hydroxyl and is then reduced by atomic hydrogen produced from HCOH. The nucleation and growth of Pd islands could occur during binding or reduction of the metal precursor or during both stages. On the basis of such ALD chemistry, several approaches were evaluated to synthesize/stabilize ultrasmall Pd particles. The effectiveness of each of these methods for the purpose of further reducing the ALD Pd particle size will be discussed below.

According to eq 1, the density of surface hydroxyls should control the number of adsorbed $Pd(hfac)_2$ precursor molecules. Although the mechanism for Pd particle formation during ALD is not yet clearly understood, the Pd aggregation is expected to increase with increasing concentration of adsorbed metal precursor species. Consequently, decreasing the surface hydroxyl density (samples 2, 3, and 7 in Table 1) should increase the distance between adjacent chemisorbed Pd species and reduce the likelihood of forming large Pd particles by the migration and merging of smaller particles.

Performing the $Pd(hfac)_2$ precursor exposures at a lower temperature might also help reduce the Pd particle size. Diffusion on metal oxide surfaces depends strongly on temperature. Therefore, dosing the $Pd(hfac)_2$ precursor at a lower temperature should inhibit the aggregation of the Pd species during the first half cycle of the ALD process. Typically, Pd ALD is carried out at 200 °C, the temperature required to remove the −hfac ligands from the attached metal precursor by atomic hydrogen dissociated from HCOH (eq 2). However, chemisorption of the $Pd(hfac)_2$ precursor to the alumina surface (eq 1) proceeds at much lower temperatures.[37] Since the $Pd(hfac)_2$ precursor bubbler was maintained at 60 °C to provide enough vapor pressure (∼20 mTorr) for coating the high surface area powder support, the ALD reactor must be maintained at a higher temperature to prevent condensation of the $Pd(hfac)_2$. For samples 4, 6, and 7 in Table 1, the $Pd(hfac)_2$ precursor exposure and purge were performed at 100 °C. The ALD reactor was then heated to 200 °C to carry out the formalin dose and purge for ligand removal.

To reduce the mobility of the deposited Pd species, ALD alumina overcoats were applied on samples 5, 6, and 7 after the $Pd(hfac)_2$ precursor but before the formalin exposures. The alumina overcoats are expected to bond to the support and the Pd particles simultaneously, thereby anchoring the Pd particles. On the other hand, the thin alumina overcoat should not completely encapsulate the Pd particles so as to diminish their catalytic activity. In our recent study, we showed that such ALD alumina overcoats can effectively prevent sintering of the Pd nanoparticles while preserving their catalytic activity.[38]

PD LOADING

The Pd loadings for samples 1−7 measured by XRF are given in Table 1. The Pd percentages are calculated using the initial catalyst mass (before ALD alumina overcoating). Compared with the sample prepared under standard conditions (sample 1), all of the samples treated to reduce the number of surface hydroxyls (samples 2, 3, and 7) showed lower Pd loadings. These results are in qualitative agreement with the hypothesis that surface hydroxyls are the attachment points for $Pd(hfac)_2$. However, annealing to 600 °C is expected to remove ∼80% of the surface hydroxyls (from 9 to 2 nm^{-2}), whereas sample 2 only shows a moderate decrease in Pd loading (∼24%).[31] The reason for this discrepancy might be that the steric hindrance of the bulky $Pd(hfac)_2$ restricts the maximum surface density of adsorbed Pd species to well below 9 nm^{-2}. In fact, the 1.6% Pd loading resulting from one Pd ALD cycle implies a surface density of only ∼1 nm^{-2} for the adsorbed Pd species, which is

dx.doi.org/10.1021/cs2000957 |ACS Catal. 2011, 1, 665–673

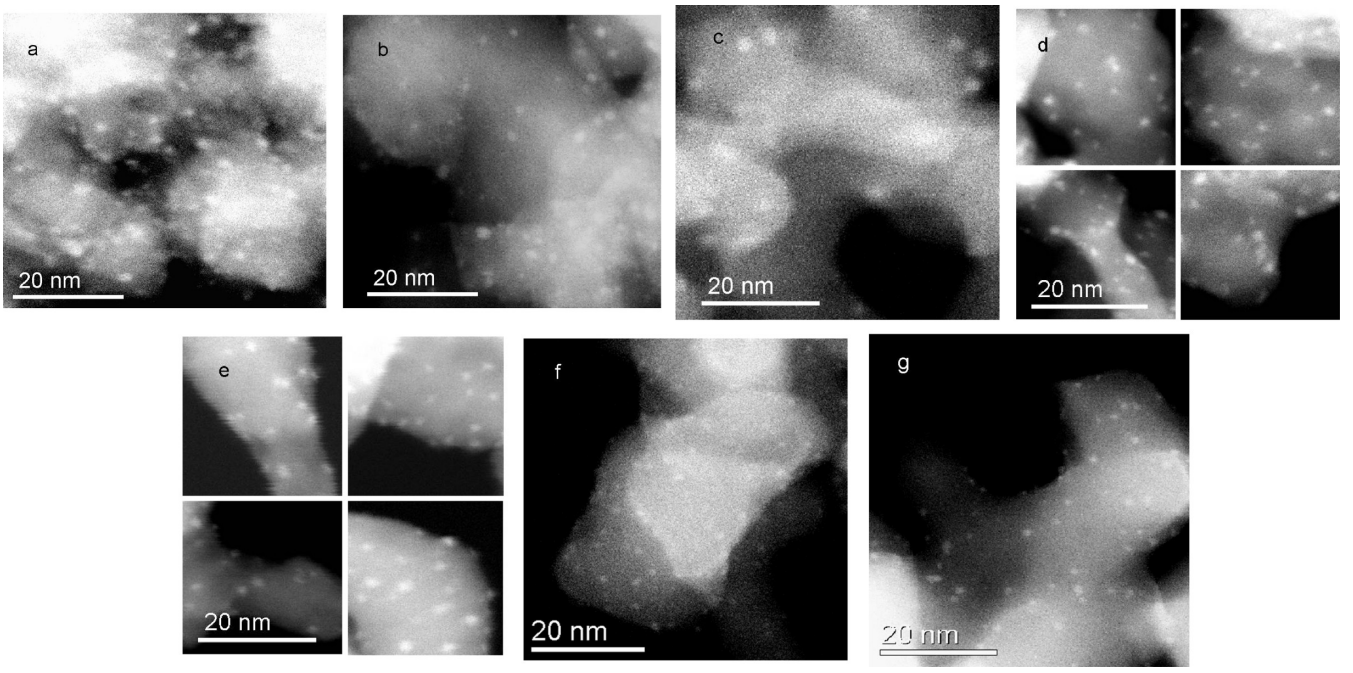

Figure 1. Representative TEM images of the ALD Pd samples: a, sample 1; b, sample 2; c, sample 3; d, sample 4; e, sample 5; f, sample 6; g, sample 7.

in accord with the size of the $Pd(hfac)_2$ molecule. Annealing to higher temperatures may further decrease the Pd loading; however, much higher temperature thermal treatments, which would likely change the alumina surface layer and support structure, were not performed. Instead, alternative low-temperature chemical methods for decreasing the surface hydroxyl concentration were investigated.

Alcohol pretreatment is expected to reduce the Pd loading, since alcohols can react with surface hydroxyls to form stable alkoxide species, which are inert to $Pd(hfac)_2$.[32,33,36] As expected, ethanol pretreatment of sample 7 reduced the Pd loading by 36% compared with sample 6. Similarly, TMA pretreatment is expected to completely remove the surface hydroxyls.[31] Although the TMA pretreatment yielded the lowest metal loading, the Pd loading on sample 3 is only 45% less than the standard, sample 1. This result suggests that $Pd(hfac)_2$ may react with the chemisorbed TMA. Adsorption on the TMA-treated alumina surface might proceed through a slow ligand exchange reaction between surface methyl groups and the $Pd(hfac)_2$ precursor, followed by decomposition of the unstable $Pd(CH_3)_x$ species.[39,40] $Pd(hfac)_2$ may also react with bridge-bonded Al−O−Al surface sites.

Since $Pd(hfac)_2$ can react with alumina hydroxyl groups at temperatures below the standard ALD conditions of 200 °C, the exposure temperature was lowered to 100 °C. At lower temperature, the Pd loading increased slightly (sample 4). This might be due to a higher hydroxyl coverage at the lower temperature or the reduced desorption of the physically adsorbed $Pd(hfac)_2$ species. The fact that sample 6, low temperature ALD plus an alumina overcoating, showed the highest Pd loading supports the latter explanation. The alumina overcoating, performed at the lower temperature for sample 6, should restrict surface diffusion necessary for the recombinative desorption of weakly bound $Pd(hfac)_2$ species, yielding a higher Pd loading.

As a method applied to confine the mobility of the adsorbed Pd species, ALD alumina overcoat itself does not affect Pd loading. As shown in Table 1, the Pd loading on the sample with the ALD alumina overcoat (sample 5) is essentially the same as the sample synthesized under standard ALD conditions (sample 1). It is reported that TMA exposure after the Pd precursor dose removes −hfac ligands from the alumina surface;[39] however, this process would not affect the loading of Pd species already attached to the surface.

PD PARTICLE SIZE AND DISPERSION

TEM was utilized to examine the morphology and size distribution of the ALD Pd particles. Figure 1a−g shows representative TEM images of Pd samples 1−7, respectively, prepared under the conditions described in Table 1. The TEM images were taken at magnifications of 400 000 and 800 000, with resolutions of 0.13 and 0.07 nm/pixel. The corresponding particle size histograms derived from these TEM images are given in Figure 2a−g, and the particle size average and standard deviation are given in Table 1. The ALD Pd particles prepared under standard conditions (sample 1) mostly ranged between 1 and 2 nm. This sample was used as a benchmark to evaluate the effectiveness of the different approaches applied to further reduce the Pd particle size.

The 600 °C preannealing of the support to reduce the hydroxyl density (sample 2) yielded a particle size distribution similar to that of sample 1 (Figures 1b and 2b). Thus, reducing the surface hydroxyl density by ∼80% leads to a decrease in the amount of chemisorbed $Pd(hfac)_2$, but only by about 25%. Contrary to what is commonly assumed, the lower metal loading and lower alumina support hydroxyl density did not lead to smaller metallic particles. Thus, thermal dehydroxylation does not appear to be an effective strategy to reduce the nanoparticle size; however, thermal treatment is effective at controlling the metal loading.

Chemical reaction of the alumina hydroxyls by pretreatment with TMA also reduced the Pd loading but produced larger Pd particles. The TEM image (Figure 1c) and corresponding histogram (Figure 2c) for sample 3 show Pd particles that are

dx.doi.org/10.1021/cs2000957 |ACS Catal. 2011, 1, 665–673

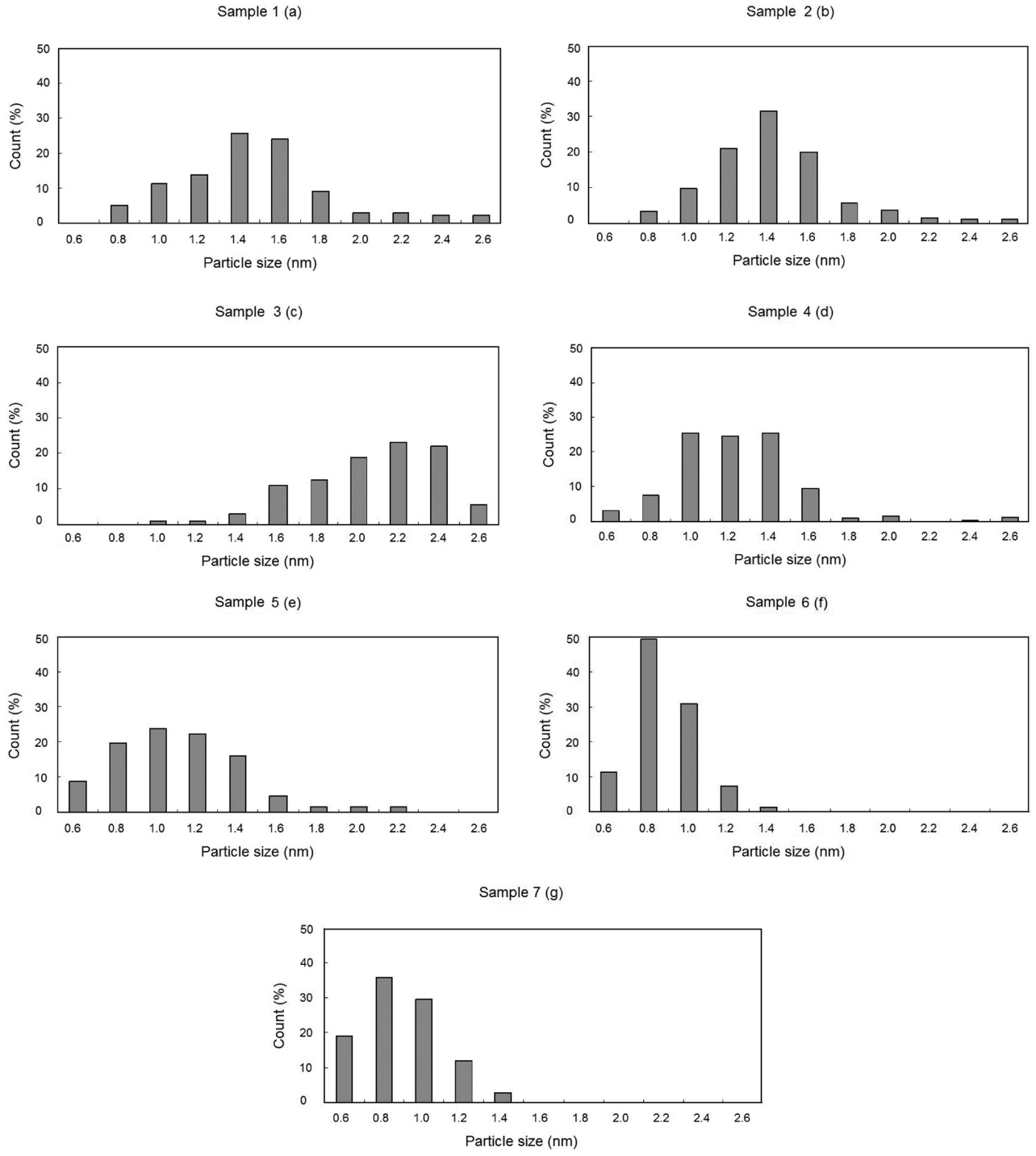

Figure 2. Particle size distribution patterns of the ALD Pd Samples: a, sample 1; b, sample 2; c, sample 3; d, sample 4; e, sample 5; f, sample 6; g, sample 7.

mostly 2 nm or larger. The formation of these large Pd particles appears to be due to the reduction and higher mobility of the Pd species. The TMA exposure prior to the $Pd(hfac)_2$ exposure will replace all the surface hydroxyls with $-Al(CH_3)_x$ species. As a result, the $Pd(hfac)_2$ precursor introduced in the following ALD cycle may undergo ligand exchange to form $Pd(CH_3)_x$ species, which subsequently decompose to produce metallic Pd.[39,40] Metallic Pd lacks strong chemical bonding to the surface and is more likely to diffuse and aggregate to form large particles. DRIFTS measurements and a dark appearance suggest the presence of Pd^0 on the alumina surface after $Pd(hfac)_2$/TMA/H_2O exposures (data not shown), indicating the possibility that surface $-Al(CH_3)_x$ groups reduce the Pd precursor. However, the detailed mechanism would require further confirmation. Due to the large particle size and the reduced metal loading, the Pd particle density on sample 3 is much lower than that of sample 1, as is clearly shown in the TEM image in Figure 1c.

Reducing the metal precursor exposure temperature to 100 °C appears to be an effective way to produce smaller Pd particles. As is shown in Figures 1d and 2d for sample 4, most of the Pd

dx.doi.org/10.1021/cs2000957 |ACS Catal. 2011, 1, 665–673

particles synthesized with the low temperature $Pd(hfac)_2$ exposure were ~0.8−1.4 nm, slightly smaller than those synthesized under the standard conditions. These results suggest that the adsorbed Pd precursor molecules are less mobile at lower temperatures, which reduces aggregation of the Pd species. However, the need to increase the temperature to 200 °C for the subsequent formalin exposure might mitigate some of the particle size reduction provided by the low temperature $Pd(hfac)_2$ exposure. Nevertheless, the slightly smaller size suggests that the temperature of the ALD dosing can be used to control the average size of ~1 nm nanoparticles.

ALD alumina overcoating to immobilize the adsorbed Pd species also appears to reduce the Pd particle size. Figures 1e and 2e show the TEM image and histogram of sample 5 prepared with two cycles of ALD alumina overcoating performed after the $Pd(hfac)_2$ exposure at 200 °C. On this sample, most of the particles are 0.8−1.4 nm, and more subnanometer particles can be observed. Since alumina ALD can be performed over a wide temperature range, we repeated the $Pd(hfac)_2$ exposure and overcoating procedure at 100 °C in an effort to minimize the Pd agglomeration. Figures 1f and 2f show the TEM image and histogram for this sample 6. The Pd particles synthesized using the low temperature ALD dosing and alumina overcoating procedure were quite small: almost all particles were <1.2 nm, and many of the particles were 0.8−1.0 nm. In addition, due to the relatively high metal loading and small particle size, the density of Pd particles on this sample is quite high. This phenomenon is desirable and a bit unusual, since for many synthesis methods, the particle size increases with metal loading.

The synthesis of sample 7 combined three methods for reducing the Pd particle size: an ethanol exposure was applied to remove a fraction of the surface hydroxyls, the $Pd(hfac)_2$ exposure was performed at 100 °C, and ALD alumina overcoating was utilized. Figures 1g and 2g demonstrate that most of these particles have the smallest average particle size (≤1.0 nm) and the size distribution is narrow, similar to that of sample 6. The particle density on sample 7 is lower than on sample 6, since the two samples have Pd particles of similar size but the metal loading of sample 7 is lower, ~36%.

TEM imaging is a direct way to determine the Pd particle size, but one needs to assume that the small volumes examined are representative of the entire sample. In contrast, EXAFS provides an estimate of the Pd particle size averaged over the entire sample through the coordination number of Pd−Pd neighbors.[41] Figure 3 presents the XANES data (Figure 3a) and k^2-weighted magnitude of the Fourier transform of the EXAFS data (Figure 3b) from the reduced samples for small (<1 nm, sample 6) and large (>2 nm, sample 3) Pd particles along with Pd foil. In Figure 3a, the position and shape of the XANES and the intensity of the first peak indicate that the Pd is fully reduced. The intensity of the magnitude of the Fourier transform indicates that these are small nanoparticles, and sample 6 is noticeably smaller than sample 3. The EXAFS fits for both spectra along with that of the sample prepared under standard conditions (sample 1) are summarized in Table 2. The Pd−Pd coordination numbers(N) for the small, medium, and large Pd particles are 5.0, 6.0, and 7.7 respectively, and the corresponding estimate of the average particles sizes are 0.8, 1.5, and 2.5 nm. The estimated average particle sizes from the EXAFS fits are in good agreement with the TEM results.

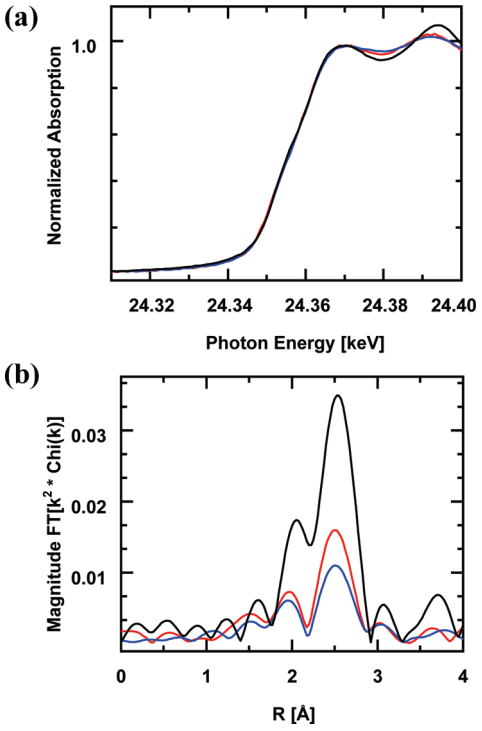

Figure 3. (a) Pd K-edge XANES from 24.30 to 24.41 keV, and (b) k^2-weighted magnitude of the Fourier transform (Δk = 2.7−11.0 Å^{-1}) of reduced Pd catalysts containing small (red, 0.8 nm, sample 6) and large (blue, 2.5 nm, sample 3) Pd particles and Pd foil (black).

Table 2. EXAFS Fitting Results for Coordination Number (N), Bond Distance (R), Debye−Waller Factor (DWF), and Energy Correction Factor (E_0) for ALD Pd Samples after Reduction[a]

sample	scatter	N	R (Å)	DWF (× 10^{-3})	E_0 (eV)	est. size (nm)
sample 1 (M)	Pd−Pd	6.0	2.75	2.0	−2.4	1.5
sample 3 (L)	Pd−Pd	7.4	2.75	2.0	−2.4	2.5
sample 6 (S)	Pd−Pd	5.0	2.75	2.0	−2.2	0.8

[a] k^2: Δk = 2.7−11.0 Å^{-1} and Δr = 1.7−2.8 Å.

The small size of the ALD Pd nanoparticles results in a high dispersion of the catalytic species on the support. The metal dispersion (fraction of surface Pd atoms) can be estimated from the particle size distribution using the model developed by Fritsche et al. and by Montejano-Carrizales et al.[42,43] Considering metal particles with cuboctahedral shape, the metal dispersion, D, can be expressed as

$$D(m) = n_{surf}/n_{total} = (30m^2 + 6)/(10m^3 + 15m^2 + 11m + 3) \quad (3)$$

where n_{surf} is the number of atoms on the surface, n_{total} is the total number of atoms, and the crust order m represents integers greater than 0, which corresponds to the particle size in terms of successive monatomic crust added to a preexisting core (m = 1 is a 13-atom cluster in which the central atom has a fully saturated 12-atom coordination, etc.).[44] On the basis of the atomic radius of Pd (R_{Pd} = 1.37 Å), the Pd particle diameter, d (in Å), can be expressed as $d(m) = 4.651\ m + 3.2$.[44] The metal

dx.doi.org/10.1021/cs2000957 |ACS Catal. 2011, 1, 665–673

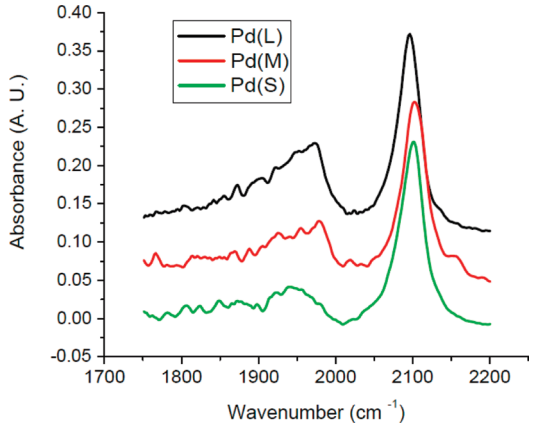

Figure 4. DRIFTS spectra of the ALD Pd samples containing large (black, sample 3), medium (red, sample 1), and small (green, sample 6) particles after CO chemisorption.

dispersion corresponding to each m value can be determined, and the overall dispersion is expressed by

$$n_{surf}/n_{total} = \sum D(d_i)\, n_{total}(d_i)/\sum n_{total}(d_i) \qquad (4)$$

In eq 4, the $n_{total}(d_i)/\Sigma\, n_{total}(d_i)$ quantities can be obtained from the particle size distributions in Figure 2. It is worth noting that eq 4 is strictly applicable only to free particles. Sometimes a correction factor (e.g., 5/6) is used to account for the atoms bound to the support that are not available for catalysis because they are buried;[44] however, this correction is not necessary for subnanometer particles that may consist of only ~10 atoms, since even the substrate-bonded atoms can participate in the catalysis. The calculated metal dispersion values are summarized in Table 1. The metal dispersion of the standard ALD Pd sample (sample 1) is 0.64. The samples prepared with low temperature metal precursor exposure followed by ALD alumina overcoating (samples 6 and 7) show the highest metal dispersions of 0.84−0.85. The samples with medium to small Pd particles (samples 2, 4, and 5) have dispersion values in the range of 0.66−0.77. The sample with the largest Pd particles (>2 nm, sample 3) has the lowest Pd dispersion of 0.50.

The nature of the Pd particle surfaces can be revealed by DRIFTS of CO chemisorbed on the Pd. Such measurements provide information on the type and availability of different facets on the Pd surface. The DRIFTS spectra of representative samples containing small (sample 6, 0.8 nm), medium (sample 1, 1.4 nm), and large (sample 3, 2.2 nm) Pd particles are shown in Figure 4. On all of the samples, we observed a sharp peak at 2090−2100 cm^{-1}, assigned to linear adsorbed CO on corner Pd atoms, and a relatively broad peak at 2000−1900 cm^{-1}, which contains two overlapped peaks assigned to μ_2 bridge-bonded CO on step/edge sites (at ~1980 cm^{-1}) and on planar Pd(111) facets (at ~1930 cm^{-1}).[45−49] Since the peak intensities represent the abundance of different types of surface sites, the relative intensity of the linear-to-bridge bonded CO (L/B ratio) reflects the ratio of the low-coordinated (corners) to higher-coordinated (edges and planes) Pd atoms and can be used as an indicator of the Pd particle size.[15] Comparing the DRIFTS spectra of the three samples, the L/B ratios increase as sample 3 (2.2 nm, L/B = 1.2) < sample 1 (1.4 nm, L/B = 2.4) < sample 6 (0.8 nm, L/B = 4.8), consistent with the decreasing Pd particle size, confirmed by the TEM and EXAFS measurements.

Because the ALD alumina overcoat might affect the CO chemisorption on Pd particles, the DRIFTS of sample 6 could be unique and is worthy of a closer look. A characteristic feature in the DRIFTS of sample 6 is that the CO IR peak at 1980 cm^{-1} is very small relative to the peak at 1930 cm^{-1}. The disappearance of the 1980 cm^{-1} peak is probably due to the preferential coverage of low-coordination Pd atoms by the ALD alumina overcoat. Our previous studies on the interaction between ALD alumina overcoats and Pd particles revealed that the thin layer of overcoat will selectively cover the Pd particles at the low coordination sites (edges and corners) while leaving the Pd (111) planes exposed.[38] Since the thin ALD alumina overcoat will partially cover the Pd atoms on the steps/edges as well as on the corners and, consequently, decrease the intensities of both associated IR peaks (the peaks at 1980 cm^{-1} and at 2090 cm^{-1}), to a similar extent, the low-coordinated-to-higher-coordinated Pd atoms ratio reflected by the L/B value obtained from the DRIFTS of sample 6 is probably even underestimated.[38] Therefore, the conclusion made on the particle size sequence based on the measured L/B ratios in the DRIFTS is not affected by reduced intensity of the 1980 cm^{-1} peak on sample 6 due to the overcoat. However, no quantitative conclusion should be drawn from these L/B values, because the IR intensities cannot be taken as absolute measure of coverage and are subject to change with characterization conditions.

CATALYTIC BEHAVIOR OF PD NANOPARTICLES

The catalytic reactions for methanol decomposition by the supported ALD Pd particles were carried out at 230−270 °C, only slightly above the sample preparation temperature, to avoid sintering of the Pd particles. Catalytic measurements were performed first on the ALD alumina-coated silica gel support, and no conversion was observed at temperatures up to 350 °C. The quantity of catalyst was adjusted to give an equal amount of Pd for each test (constant space velocity). Experimental data were collected beginning after 20 min to allow the catalysts to stabilize. The catalysts were continuously tested for 3 h at each temperature, and no deactivation was observed during the experiments. The conversions as a function of temperature for the small (sample 6, 0.8 nm), medium (sample 1, 1.4 nm), and large (sample 3, 2.2 nm) Pd particle catalysts are plotted in Figure 5a. The reproducibility of the catalysis data was within ±5% and is represented by the error bars in Figure 5. In all measurements, CO and H_2 were the only products detected and accounted for 100% (± 3%) of the carbon and hydrogen balance.

Since all the catalysis experiments were performed at the same space velocity (moles of methanol per gram of Pd), the conversion plots in Figure 5a also represent the specific activities of the different catalyst samples normalized by the total amount of supported Pd. The activities of these ALD Pd catalysts increase in sequence Pd (L) < Pd (M) < Pd (S). The TOFs of the Pd nanoparticle catalysts were calculated by normalizing the activity by the Pd metal dispersion listed in Table 1, and the results are presented in Figure 5b. Considering the metal dispersion factor, the TOFs of the small (subnanometer) and medium Pd particles are comparable and are 2× higher than the large nanoparticles.

It is generally believed that smaller Pd particles are more active for methanol decomposition. Saitoh et al. reported that in the size range of 3−6 nm, the activity of the Pd/alumina catalyst decreased rapidly with increasing particle size.[50] To some extent, our data are in line with this trend in that the activities of the small

dx.doi.org/10.1021/cs2000957 |ACS Catal. 2011, 1, 665–673

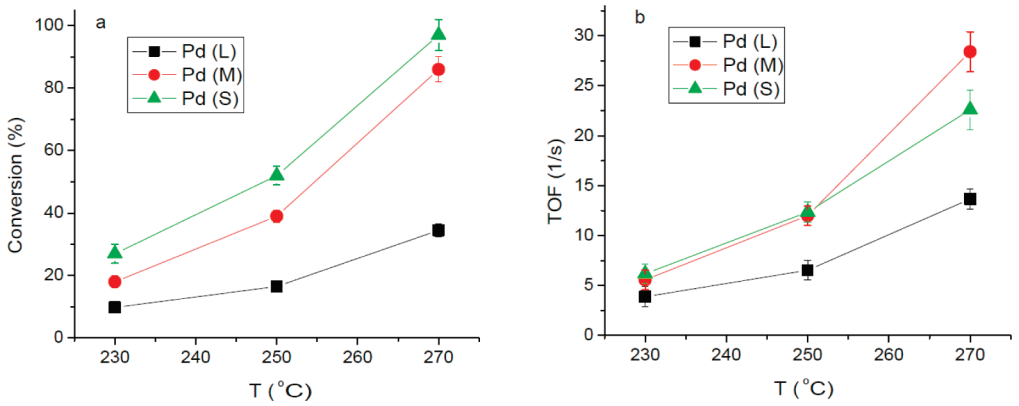

Figure 5. Conversion (a) and TOF (b) plots of the ALD Pd samples containing small (sample 6), medium (sample 1), and large (sample 3) particles measured in methanol decomposition.

ALD Pd particles are significantly higher than those of catalysts containing larger Pd particles synthesized by traditional methods (wet impregnation, sol−gel, etc.), as reported in the literature.[20] On the other hand, the TOF changed by only a factor of ∼2 as the Pd particle size was reduced from ∼2.2 to ∼1.4 nm, and no further increase in activity occurs as the particle size decreases to about 0.8 nm. For the methanol decomposition reaction, the presence of cationic Pd species (most likely Pd^{+}) as a result of the strong metal−support interaction is sometimes invoked to explain the higher activities of smaller Pd particles supported on TiO_2 or ZrO_2;[51−55] however, in our Pd/alumina system, the XANES studies showed no detectable Pd^{+} formation. Furthermore, there was no evidence for strong Pd−Al bonding in the EXAFS fitting of the ALD Pd samples.

In summary, our experimental data indicate that in methanol decomposition, the activities of the ALD Pd/alumina nanoparticle catalysts are all similar in the sub-2 nm range. However, the high Pd dispersion resulting from a smaller particle size can better utilize the expensive noble metal catalyst. Although the rate of methanol decomposition does not appear to be highly dependent on Pd nanoparticle size, many reactions are size-dependent, that is, structure-sensitive.[56,57] The ability to precisely control the average particle size while giving narrow particle size distributions in this critical small subnanometer size range will allow for these effects to be more effectively studied. It is worth noting that in the methanol decomposition reaction, the alumina overcoating does not reduce the catalytic activity because the catalytically active Pd(111) facets remain bare.[38] This will probably not hold true for all reactions, and thus, the alumina overcoating may reduce the activity for some reactions. On the other hand, the overcoating material might actually enhance certain reactions by exerting a support effect. Therefore, when applying the ALD overcoating technique to synthesize and stabilize nanoparticle catalysts, factors such as the interaction between the catalyst and the coating material, and the thickness of the overcoat layer will require special considerations.

CONCLUSIONS

Different approaches were explored to synthesize ultrasmall Pd particles by modifying the conventional Pd ALD process. These methods included pretreatments to reduce the surface hydroxyl density, executing the $Pd(hfac)_2$ precursor exposures at lower temperature, applying ALD alumina overcoating layers, and combinations of these procedures. TEM measurements showed that manipulating the hydroxyl density on the support mostly affected the metal loading rather than reducing the particle size. Moreover, complete removal of the surface hydroxyls by TMA pretreatment produced unusually large (>2 nm) Pd nanoparticles. Both low-temperature $Pd(hfac)_2$ exposures and protective ALD alumina overcoating helped generate smaller metal particles, and monodispersed, subnanometer Pd particles could be synthesized by combining these two procedures. The ultrasmall size of the Pd particles synthesized by these methods was verified by EXAFS measurements. The peak intensities of linear to bridge-bonded CO in DRIFTS measurements indicated a particle size sequence consistent with the TEM and EXAFS results. The catalytic performances of the ALD Pd particles with different sizes were compared using the methanol decomposition reaction. The specific activities of the ultrasmall (<1 nm), medium (1−2 nm), and large (>2 nm) Pd catalyst particles increase in the sequence Pd (L) < Pd (M) < Pd (S). Considering the metal dispersion, the TOFs for the three samples were Pd (L) < Pd (S) ∼ Pd (M). The TOF of the small and medium Pd particles was higher than that of the larger ones by a factor of only 2, indicating that in methanol decomposition, the activities of the ALD Pd/alumina nanoparticle catalysts are all similar in the sub-2 nm range.

AUTHOR INFORMATION

Corresponding Author
*E-mail: jelam@anl.gov.

ACKNOWLEDGMENT

This work was supported in part by the U.S. Department of Energy, BES-HFI, Chemical Sciences under Contract DE-AC-02-06CH11357 and by The Dow Chemical Company under the Dow Methane Challenge Award. The TEM work was supported as part of the Institute for Atom-efficient Chemical Transformations (IACT), an Energy Frontier Research Center funded by the U.S. Department of Energy, Office of Science, Office of Basic Energy Sciences. The use of the Advanced Photon Source was supported by the U.S. Department of Energy, Office of Science, Office of Basic Energy Sciences, under Contract No. DE-AC02-06CH11357. Materials Research Collaborative Access Team (MRCAT, Sector 10 ID) operations are supported by the Department of Energy and the MRCAT member institutions.

REFERENCES

(1) Astruc, D. *Inorg. Chem.* **2007**, *46*, 1884–1894.
(2) Astruc, D. *Nanoparticles and Catalysis*. Wiley-VCH: New York, 2008.
(3) Bell, A. T. *Sci.* **2003**, *299*, 1688–1691.
(4) Chen, M. S.; Goodman, D. W. *Catal. Today* **2006**, *111* (1−2), 22–33.
(5) Boutonnet, M.; Lögdberg, S.; Svensson, E. E. *Curr. Opin. Colloid Interface Sci.* **2008**, *13* (4), 270–286.
(6) Cuenya, B. R. *Thin Solid Films* **2010**, *518* (12), 3127–3150.
(7) Aiken, J. D.; Finke, R. G. *J. Mol. Catal.* **1999**, *145* (1−2), 1–44.
(8) Liu, W. *Chin. Particuology* **2005**, *3* (6), 383–394.
(9) Summers, J. C.; Ausen, S. A. *J. Catal.* **1978**, *52* (3), 445–452.
(10) Toebes, M. L.; van Dillen, J. A.; de Jong, K. P. *J. Mol. Catal. A: Chem.* **2001**, *173* (1−2), 75–98.
(11) Ogasawara, S.; Kato, S. *J. Am. Chem. Soc.* **2010**, *132* (13), 4608–4613.
(12) Liu, Q.; Bauer, J. C.; Schaak, R. E.; Lunsford, J. H. *Angew. Chem., Int. Ed.* **2008**, *47*, 6221–6224.
(13) Ho, P.-F.; Chi, K.-M. *Nanotechnology* **2004**, *15*, 1059–1064.
(14) Yuranov, I.; Moeckli, P.; Suvorova, E.; Buffat, P.; Kiwi-Minsker, L.; Renken, A. *J. Mol. Catal. A: Chem.* **2003**, *192*, 239–251.
(15) Fu, B.; Missaghi, M. N.; Downing, C. M.; Kung, M. C.; Kung, H. H.; Xiao, G. *Chem. Mater.* **2010**, *22*, 2181–2183.
(16) Pileni, M.-P. *Nat. Mater.* **2003**, *2*, 145–150.
(17) Hernandez, J.; Solla-Gullon, J.; Herrero, E. J. *Electroanal. Chem.* **2004**, *574*, 185–196.
(18) Wilson, O. M.; Scott, R. W.; Garcia-Martinez, J. C.; Crooks, R. M. *J. Am. Chem. Soc.* **2005**, *127*, 1015–1024.
(19) Borodko, Y.; Humphrey, S. M.; Tilley, T. D.; Frei, H.; Somorjai, G. A. *J. Phys. Chem. C.* **2007**, *111*, 6288–6295.
(20) Feng, H.; Elam, J. W.; Libera, J. A.; Setthapun, W.; Stair, P. C. *Chem. Mater.* **2010**, *22*, 3133–3142.
(21) Setthapun, W.; Williams, W. D.; Kim, S. M.; Feng, H.; Elam, J. W.; Rabuffetti, F.; Poppelmeier, K.; Stair, P. C.; Stach, E.; Fabio, R.; Miller, J.; Marshall, C. *J. Phys. Chem. C.* **2010**, *144* (21), 9758–9771.
(22) Christensen, S. T.; Feng, H.; Libera, J. A.; Neng, G.; Miller, J. T.; Stair, P. C.; Elam, J. W. *Nano Lett.* **2010**, *10* (8), 3047–3051.
(23) Vuoria, H.; Lindbladb, M.; Outi, A.; Krausea, I. *Stud. Surf. Sci. Catal.* **2006**, *162*, 505–512.
(24) Li, J.; Liang, X.; King, D. M.; Jiang, Y.; Weimer, A. W. *Appl. Catal., B* **2010**, *97* (1−2), 220–226.
(25) King, J. S.; Wittstock, A.; Biener, J.; Kucheyev, S. O.; Wang, Y. M.; Baumann, T. F.; Giri, S. K.; Hamza, A. V.; Baeumer, M.; Bent, S. F. *Nano Lett.* **2008**, *8* (8), 2405–2409.
(26) Elam, J. W.; Libera, J. A.; Huynh, T. H.; Feng, H.; Pellin, M. J. *J. Phys. Chem. C* **2010**, *114*, 17286–17292.
(27) Doering, R.; Nishi, Y., *Handbook of Semiconductor Manufacuring Technology*. CRC Press: Boca Raton, FL, 2008.
(28) Lee, S.; Lee, B.; Mehmood, F.; Seifert, S.; Libera, J. A.; Elam, J. W.; Greeley, J.; Zapol, P.; Curtiss, L. A.; Pellin, M. J.; Stair, P. C.; Winans, R. E.; Vajda, S. *J. Phys. Chem. C* **2010**, *114*, 10342–10348.
(29) Zhu, Y.; Peng, S.-C.; Emi, A.; Su, Z.; Monalisa, K. R. A. *Adv. Synth. Catal.* **2007**, *349*, 1917–1922.
(30) Elam, J. W.; Groner, G. M.; George, S. M. *Rev. Sci. Instrum.* **2002**, *73* (8), 2981–2987.
(31) Puurunen, R. L. *J. Appl. Phys.* **2005**, *97*, 121301–121352.
(32) Golay, S.; Doepper, R.; Renken, A. *Appl. Catal., A* **1998**, *172*, 97–106.
(33) Knozinger, H.; Stubner, B. *J. Phys. Chem.* **1978**, *82* (13), 1526–1532.
(34) Elam, J. W.; Zinovev, A.; Han, C. Y.; Wang, H. H.; Welp, U.; Hryn, J. N.; Pellin, M. J. *Thin Solid Films* **2006**, *515*, 1664–1673.
(35) Dafinov, A.; Garcia-Valls, R.; Font, J. *J. Membr. Sci.* **2002**, *196*, 69–77.
(36) Yanguas-Gil, A.; Elam, J. W. *ECS Trans.* **2010**, *33* (2), 333–342.
(37) Lu, J.; Stair, P. C. *Angew. Chem., Int. Ed.* **2010**, *49*, 2547–2551.
(38) Feng, H.; Lu, J.; Stair, P. C.; Elam, J. W. *Catal. Lett.* **2011**, *141*, 512−517.
(39) Goldstein, D. N.; George, S. M. *Appl. Phys. Lett.* **2009**, *95*, 143106.
(40) Low, J. J.; Goddard, W. A. *Organometallics* **1986**, *5* (4), 609–622.
(41) Miller, J. T.; Kropf, A. J.; Zha, Y.; Regalbuto, J. R.; Louis, L.; Bus, E.; Van Bokhoven, J. A. *J. Catal.* **2006**, *240*, 222–234.
(42) Fritsche, H. G.; Benfield, R. E. Z. *Phys. D: At. Mol. Clusters* **1993**, *26*, S15–S17.
(43) Montejano-Carrizales, J. M.; Aguilera-Granja, F.; Moran-Lopez, J. L. *Nanostruct. Mater.* **1997**, *8*, 269–287.
(44) Agostini, G.; Pellegrini, R.; Leofanti, G.; Bertinetti, L.; Bertarione, S.; Groppo, E.; Zecchina, A.; Lamberti, C. *J. Phys. Chem. C* **2009**, *113*, 10485–10492.
(45) Lear, T.; Marshall, R.; Lopez-Sanchez, J. A.; Jackson, S. D.; Klapotke, T. M.; Baumer, M.; Rupprecheter, G.; Freund, H. J.; Lennon, D. *J. Chem. Phys.* **2005**, *123*, 174706.
(46) Baumer, M.; Libuda, J.; Neyman, K. M.; Rosch, N.; Rupprechter, G.; Freund, H.-J. *Phys. Chem. Chem. Phys.* **2007**, *9*, 3541–3558.
(47) Schauermann, S.; Hoffmann, J.; Johanek, V.; Hartmann, J.; Libuda, J.; Freund, H.-J. *Catal. Lett.* **2002**, *84* (3−4), 209–217.
(48) Schauermann, S.; Hoffmann, J.; Johánek, V.; Hartmann, J.; Libuda, J. *Phys. Chem. Chem. Phys.* **2002**, *4*, 3909–3918.
(49) Wolter, K.; Seiferth, O.; Kuhlenbeck, H.; Baumer, M.; Freund, H.-J. *Surf. Sci.* **1998**, *399*, 190–198.
(50) Saitoh, Y.; Ohtsu, S.; Makie, Y.; Okada, T.; Satoh, K.; Tsuruta, N.; Terunuma, Y. *Bull. Chem. Soc. Jpn.* **1990**, *63* (1), 108–115.
(51) Matsumura, Y.; Okumura, M.; Usami, Y.; Kagawa, K.; Yamashita, H.; Anpo, M.; Haruta, M. *Catal. Lett.* **1997**, *44*, 189–191.
(52) Matsumura, Y.; Shen, W. *Top. Catal.* **2003**, *22* (3−4), 271–275.
(53) Nag, N. K. *Catal. Lett.* **1994**, *24*, 37–46.
(54) Sun, K.; Liu, J.; Nag, N.; Browning, N. D. *Catal. Lett.* **2002**, *84* (3−4), 193–199.
(55) Seshu Babu, N.; Lingaiah, N.; Gopinath, R.; Reddy, P. S. S.; Prasad, P. S. S. *J. Phys. Chem. C* **2007**, *111*, 6447–6453.
(56) Che, M.; Bennett, C. O. *Adv. Catal.* **1989**, *36*, 55–172.
(57) Wilson, O. M.; Knecht, M. R.; Garcia-Martinez, J. C.; Crooks, R. M. *J. Am. Chem. Soc.* **2006**, *128* (14), 4510–4511.